Available online at www.sciencedirect.com

SciVerse ScienceDirect

Ceramics International 39 (2013) 4597–4607

CERAMICS INTERNATIONAL

www.elsevier.com/locate/ceramint

Microstructure and wear behavior of spark plasma sintered Ti_3SiC_2 and Ti_3SiC_2–TiC composites

Nidul C. Ghosh, Sandip P. Harimkar*

School of Mechanical and Aerospace Engineering, Oklahoma State University, Stillwater, OK 74078, United States

Received 13 October 2012; received in revised form 20 November 2012; accepted 20 November 2012
Available online 7 December 2012

Abstract

In this paper, processing of Ti_3SiC_2 and Ti_3SiC_2–TiC composites from Ti/Si/TiC/Al powder using spark plasma sintering (SPS) at 1250 °C is reported. The TiC content in the starting powder mixture was optimized such that the resultant Ti_3SiC_2–TiC composites retained up to 30 vol% excess TiC as reinforcement. The phase content of TiC reinforcement in the composites, calculated from x-ray diffraction analysis, is compared with TiC content in excess of stoichiometric TiC content needed for the formation of Ti_3SiC_2. The results indicate that the composition of the SPS sintered Ti_3SiC_2–TiC composites (relative percentages of Ti_3SiC_2 matrix and TiC reinforcement content) can be effectively tailored by optimum design of the composition of starting powder mixture. The effect of TiC reinforcement content on relative density, phase development, microstructure, hardness, and friction and wear behavior of Ti_3SiC_2 and Ti_3SiC_2–TiC composites are presented.

Keywords: A. Sintering; B. Microstructure; C. Hardness; C. Wear Resistance

1. Introduction

Ti_3SiC_2 ternary carbide exhibits remarkable combination of properties of both ceramics and metallic materials, and for this reason, it is often referred to as ductile ceramic. Ti_3SiC_2 is elastically stiff, electrically and thermally conductive, high temperature oxidation and chemical attack resistant, damage tolerant, thermal shock resistant, and also machinable material. It also has relatively lower density, hardness, and thermal expansion coefficient [1–3]. Ti_3SiC_2 is a promising material for high temperature applications such as engine cylinders and electrical contacts. Ti_3SiC_2 has comparable strength, higher corrosion resistance, and nearly half the density of nickel- and cobalt-based superalloys currently being used in engine cylinder applications [4]. The copper and silver-based electrical contacts have been used for small and medium current loads because of their excellent electrical and mechanical properties. However, under heavy loads applications, the uses of copper- and silver-based contacts are limited due to the formation of oxide films and corrosion products and also due to the danger of welding in presence of high current flow and arc formation. The use of Ti_3SiC_2 is expected to improve the material performance in these applications because of its high melting temperature and also excellent high temperature oxidation and corrosion resistance. The engine cylinder walls and electrical contacts are often found to be sensitive to wear. Although the basal planes of Ti_3SiC_2 exhibit very low friction coefficient [5], the polycrystalline Ti_3SiC_2 demonstrated a high steady state friction coefficient value of 0.83 due to their layered structure [6]. Due to relatively low hardness and good ductility, the polycrystalline Ti_3SiC_2 also exhibits significant wear weight loss. Several publications reported incorporation of hard secondary phases (Al_2O_3, TiB_2, 3Y-TZP) in Ti_3SiC_2 matrix to improve hardness and wear resistance of these composites [7–9]. The processing and characterization of composites of Ti_3SiC_2 with corresponding binary carbides (TiC and SiC) have also been reported in recent publications. Most of the investigations focused on Ti_3SiC_2–SiC composites reported improvements in hardness and wear resistance over monolithic Ti_3SiC_2 [10,11]. While damage tolerance, hardness, thermal shock resistance and high temperature oxidation resistance of the composites were reported to be improved in presence of SiC, the fracture toughness was decreased reportedly due to

*Corresponding author. Tel.: +1 405 744 5830, +1 405 744 5900.
E-mail address: sandip.harimkar@okstate.edu (S.P. Harimkar).

0272-8842/$ - see front matter © 2012 Elsevier Ltd and Techna Group S.r.l. All rights reserved.
http://dx.doi.org/10.1016/j.ceramint.2012.11.058

thermal expansion mismatch between Ti_3SiC_2 (8.6×10^{-6}/K, a-direction and 9.7×10^{-6}/K, *c*-direction) [12], and SiC (5.12×10^{-6}/K) [13–15]. On the other hand, TiC, with higher hardness (28–35 GPa), stiffness (Young's modulus about 410–510 GPa), better temperature stability (melting point of 3067 °C) than SiC, and thermal expansion coefficient (7.4×10^{-6}/K for TiC) closer to that of Ti_3SiC_2 [13], seems to be a more suitable reinforcement for Ti_3SiC_2. Hu et al. reported on densification of Ti_3SiC_2–TiC (30 vol%) and Ti_3SiC_2–SiC (30 vol%) composites [15]. The processing of Ti_3SiC_2–TiC composite was carried out using mechanical alloying followed by hot pressing (MA–HP) or hot pressing of powder blend (MIX-HP). More uniform distribution of phases was achieved with MA–HP process than with MIX-HP process [16]. Zhang et al. also reported spark plasma sintering (SPS) of Ti_3SiC_2–TiC composites (reinforced with 0–40 vol% TiC) from Ti, C, Si, and Al powder mixtures in the temperature range of 1250–1350 °C [17]. The authors also reported refinement of Ti_3SiC_2 matrix grains and associated increase in hardness up to 13 GPa with increasing TiC reinforcement content. The fracture toughness and flexural strength also improved with TiC reinforcement, except for composites with 40 vol% TiC. The processing of Ti_3SiC_2–TiC composites (with up to 90 vol% TiC) from Ti/Si/TiC powder mixture using SPS sintering in the temperature range of 1250–1400 °C has also been reported [18]. The composites with 10 vol% TiC content showed best densification effect. The flexural strength of the composites increased progressively with increasing TiC content up to 50 vol% and then decreased towards high end of TiC reinforcement content. As the formation of Ti_3SiC_2 is often accompanied with large amount of undesired ancillary TiC phase, the final TiC reinforcement content in the composites is expected to be higher than excess TiC used in starting powder. In the previous literature, the resultant TiC content in the composites was found to be lower than excess TiC content in the powder mixture (desired level of reinforcement) [18,19]. Such discrepancies in results of Ti_3SiC_2–TiC composites require further investigation in this field. Again, while numerous papers deal with microstructural evolution and mechanical characterization of Ti_3SiC_2–TiC composites, reports on wear behavior of Ti_3SiC_2–TiC composites are very limited. Understanding of wear behavior of Ti_3SiC_2–TiC composites is very important for the development of engineering components with improved wear performance. In this paper, spark plasma sintering (SPS) of Ti_3SiC_2 and Ti_3SiC_2–TiC composites (reinforced with up to 30 vol% TiC) from Ti_3SiC_2 is reported. The Ti_3SiC_2–TiC composites were formed by adding additional TiC in starting powder mixture in excess of stoichiometric TiC content needed for the formation of Ti_3SiC_2. Systematic investigations on effect of TiC reinforcement content on relative density, phase development, microstructure, hardness, and friction and wear behavior of Ti_3SiC_2 and Ti_3SiC_2–TiC composites are presented.

2. Experimental procedure

For the preparation of single phase Ti_3SiC_2 and Ti_3SiC_2–TiC composites, commercially available Ti (<44 μm), Si (<1.5 μm), and TiC (<2 μm) powders were mixed according to the equation:

$$Ti + Si + xTiC = Ti_3SiC_2 + (x-2)TiC \quad (1)$$

Also, 0.2 mol of Al (<2 μm) was added to the mixture to minimize the amount of auxiliary TiC in the sintered samples. Al removes TiC impurity by forming minor interfacial liquid phase which favors diffusion of Ti and C atoms into the system [20]. The starting powder mixtures were weighed to synthesize target composition of 0 (TSC), 10 (TC10), 20 (TC20), and 30 (TC30) vol% TiC reinforced Ti_3SiC_2 composites. The relative weight percentages of powder constituents to obtain desired levels (0–30 vol%) of TiC reinforcement in the Ti_3SiC_2–TiC composites are given in Table 1. The powder mixtures were dry milled in a high energy planetary ball mill (Fritsch) using tungsten carbide milling media. The powder mixtures were milled for 1 h with a mixing speed of 500 rpm and ball to powder ratio of 8:1. The powder mixtures were then filled into graphite molds of 20 mm diameter for SPS sintering at 1250 °C with sintering pressure of 50 MPa, soaking time of 15 min, and heating rate of 100 °C/min (Thermal Technology, Inc). X-ray diffraction (XRD) analysis of the SPS sintered samples was conducted using a Philips Norelco x-ray diffractometer operating with Cu K_α radiation ($\lambda = 1.54178$ Å) at 45 kV and 40 mA. X-ray analysis was used for the identification of constituent phases and their relative percentages in the sintered samples. The relative density of the synthesized Ti_3SiC_2 and Ti_3SiC_2–TiC composites was measured based on Archimedes' principle using density measurement instrument (Mettler Toledo). A scanning electron microscope (JEOL) equipped with energy dispersive x-ray spectroscopy (EDS) detector was used for microstructural and compositional (elemental) analysis. Microhardness of

Table 1
Weight percentages of powder constituents to obtain desired levels (0–30 vol%) of TiC reinforcement in the Ti_3SiC_2–TiC composites.

Sample	*Weight percentage* (*wt*%)				*Theoretical TiC* (*vol*%)	*Measured density* (g/cm^3)
	Ti	Si	TiC	Al		
TSC	23.82	13.97	59.60	2.61	0	4.510
TC10	21.31	12.50	63.85	2.34	10	4.503
TC20	18.83	11.05	68.05	2.07	20	4.471
TC30	16.38	9.61	72.20	1.81	30	4.468

the composites was measured using a Vickers hardness tester (Clark Instruments) operated with a normal force of 9.8 N and dwell time of 15 s. Dry (unlubricated), room temperature sliding wear tests were performed on the samples using a ball-on-disk test system (Nonovea). A 6 mm diameter silicon nitride (Si_3N_4) ball was used as a counter body against the polished surfaces of the sintered samples. Each wear test was performed with a constant load of 10 N for total test duration of 60 min (12,000 cycles). After every 10 min interval, weight loss was measured. Each experiment was repeated three times and an average value and standard deviation for wear weight loss were reported. A non-contact optical 3D profilometer (Nanovea) was used for analyzing the depth profiles across the wear tracks. The microstructure of worn surfaces was analyzed using SEM.

3. Results and discussion

3.1. XRD analysis of powders and sintered Ti_3SiC_2–TiC composites

Fig. 1 shows the x-ray diffraction (XRD) patterns from starting powders after 1 h of ball milling. The XRD patterns showed intense peaks for TiC and also peaks of Si and Ti. Note that TiC, Si, and Ti were the constituents in the starting powder. The intensity of TiC peaks increased and that of Si and Ti peaks decreased with increasing TiC content from TSC (0% TiC) to TC30 (30% TiC) samples. As the peaks for all major constituents of the starting powder were observed in the XRD patterns, the results indicate that no solid state reactions between any constituent phases occurred after ball milling. The purpose of ball milling was to get the uniform distribution of constituent phases in the mixture before SPS sintering. In particular, no peaks for Ti–Si alloy were found in XRD suggesting Si and Ti did not form any solid solution or intermediate phases at this milling condition. XRD patterns of the samples sintered by SPS are presented in Fig. 2. Clearly, Ti and Si peaks disappeared after SPS

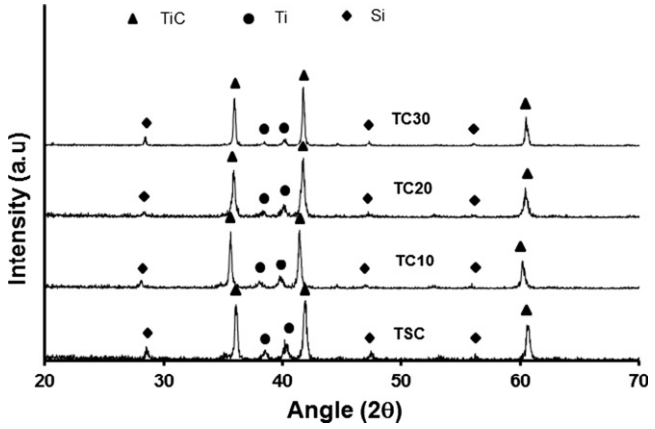

Fig. 1. XRD patterns from mechanically milled powders used for SPS sintering of Ti_3SiC_2 (TSC) and Ti_3SiC_2–TiC (TC10, TC20, and TC30) composites.

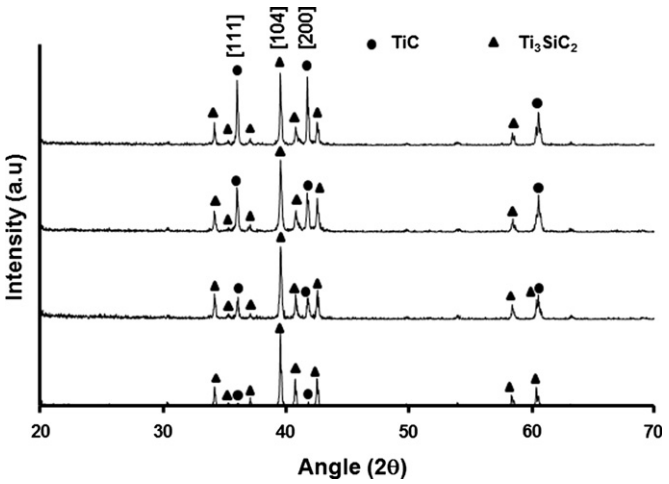

Fig. 2. XRD patterns from Ti_3SiC_2 (TSC) and Ti_3SiC_2–TiC (TC10, TC20, and TC30) composites SPS sintered at 1250 °C.

sintering. Also, peaks corresponding to intermediate phases such as titanium silicides ($TiSi_2$ and Ti_5Si_3) were not observed suggesting complete reaction at these sintering parameters (sintering temperature of 1250 °C). The peaks only corresponding to newly formed Ti_3SiC_2 phase along with TiC can be seen in the XRD patterns. For TSC samples, with theoretical TiC content of 0 vol%, very low intensity TiC peaks can be seen in the background suggesting retention of small quantity of minor phase TiC. For the new phase Ti_3SiC_2, peak corresponding to (104) plane at $2\theta = 39.615^\circ$ remains the most intense peak. This is also the most intense peak for the standard randomly oriented polycrystalline Ti_3SiC_2 (JCPDS ID: 48-1826), suggesting that the SPS sintering of ball milled constituent powders does not result any preferred crystallographic texture in the newly formed Ti_3SiC_2 phase. However, the peaks corresponding to (111) and (200) planes of TiC become increasingly intense with increasing TiC content from TSC to TC30 samples. To compare the TiC content in the SPS sintered samples with the desired theoretical TiC content (content in excess of stoichiometric TiC needed for the formation of Ti_3SiC_2), quantitative XRD analysis was conducted. The quantitative XRD analysis was conducted using calibrated standard additive method developed by Zhang et al. for these compositions [12]. For this analysis, intensities of representative (200) reflection of TiC at $2\theta = 41.74^\circ$ and (104) reflection of Ti_3SiC_2 at $2\theta = 39.548^\circ$ were used. The relative amount (vol%) of TiC in the Ti_3SiC_2–TiC composites is given by:

$$V_{TiC} = \frac{I_{TiC}/I_{Ti_3SiC_2}}{1.95 + I_{TiC}/I_{Ti_3SiC_2}} \quad (2)$$

The relative amounts of theoretical TiC (content in excess of stoichiometric TiC needed for the formation of Ti_3SiC_2) and calculated TiC (from XRD analysis) are compared in Fig. 3. It can be seen that the XRD-calculated TiC content is about 1–3% higher than the desired theoretical TiC content of the Ti_3SiC_2–TiC

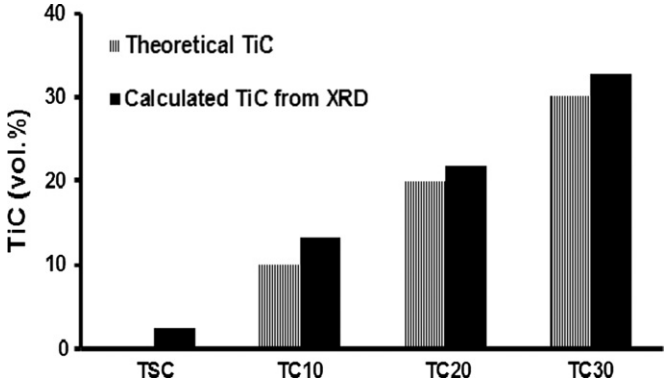

Fig. 3. Relative amounts of theoretical TiC (content in excess of stoichiometric TiC needed for the formation of Ti_3SiC_2) and calculated TiC (from XRD analysis) for SPS sintered Ti_3SiC_2 (TSC) and Ti_3SiC_2–TiC (TC10, TC20, and TC30) composites.

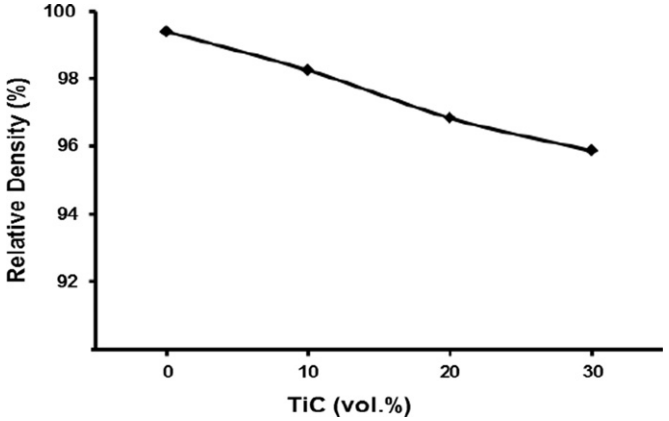

Fig. 4. Relative densities of the Ti_3SiC_2–TiC composites as a function of TiC reinforcement content.

composites. While overestimation of TiC content could be due to errors in the calibration method used for quantitative analysis, this could also be due to non-uniform reaction (due to temperature gradient during SPS sintering) resulting in higher amounts of TiC (unreacted TiC or as one of the decomposition products of Ti_3SiC_2). Previous reports have shown that the temperature gradient of about 25–50 °C can be readily established during SPS sintering. However, in general, the theoretical (based on stoichiometry) and calculated (XRD analysis) TiC contents are relatively closer suggesting that reinforcement content in the SPS sintered Ti_3SiC_2–TiC composites can be effectively controlled by adding excess TiC in the stoichiometric composition of Ti/Si/TiC powder mixture.

3.2. Relative density and microstructure

The variation of relative densities of SPS sintered Ti_3SiC_2 and Ti_3SiC_2–TiC composites with TiC reinforcement content in shown in Fig. 4. The theoretical density of the composites, used for obtaining relative densities, was calculated using a rule of mixture using the densities of two constituent phases ($\rho_{Ti_3SiC_2} = 4.53$ g/m^3 and $\rho_{TiC} = 4.93$ g/m^3). With the given SPS processing parameters, the TSC samples (nearly single phase Ti_3SiC_2) exhibited best densification with relative density greater than 99%. With the similar SPS processing parameters, the relative density of the Ti_3SiC_2–TiC composites decreased with increasing TiC reinforcement content. The Ti_3SiC_2–TiC composites with 30 vol% TiC exhibited relative density of about 95%. Clearly, the TiC reinforcement makes the densification of Ti_3SiC_2–TiC composites more difficult. This seems to be direct consequence of higher melting point of TiC ($T_m \sim 3160$ °C) compared to that of Ti_3SiC_2 ($T_m \sim 3000$ °C). Yang et al. reported processing of Ti_3SiC_2 from Ti–Si–TiC powder mixture in the temperature range of 700–1200 °C [21]. XRD analysis indicated formation of new intermediate phase Ti_5Si_3 from the reaction between Ti and Si while the intensities of TiC peaks remained unchanged. The unaltered TiC requires higher sintering temperature for full densification. Teber et al. reported SPS sintering of TiC in the temperature range of 1350–1800 °C with a pressure of 80 MPa and soaking time of 5 min [22]. At lower sintering temperature of 1350 °C, the sintered TiC samples exhibited significant open porosity. Near full densification of TiC with relative density of 99.4% was obtained for sintering temperature of 1800 °C. In this investigation, the sintering temperature (1250 °C) and pressure (50 MPa) used were significantly lower than those used in these previous reports, resulting in lower relative densities of the Ti_3SiC_2–TiC composites at higher TiC reinforcement content. Better densification in Ti_3SiC_2–TiC composites with higher TiC reinforcement content can potentially be achieved with increasing SPS sintering temperature. However, our previous results have indicated that Ti_3SiC_2 starts decomposing into TiC and other auxiliary phases above 1300 °C. It is important to select optimum sintering temperature for better densification without any decomposition of matrix phase in Ti_3SiC_2–TiC composites with higher TiC reinforcement content.

SEM micrographs from polished and etched surfaces of SPS sintered Ti_3SiC_2 and Ti_3SiC_2–TiC composites are presented in Fig. 5. For the Ti_3SiC_2 sample (Fig. 5a), the microstructure showed fine plate shaped and coarse blocky grains of Ti_3SiC_2 and also bright precipitate-like agglomerates. EDS elemental maps corresponding to elements Al, Si, and Ti for this TSC sample are shown in Fig. 6 (EDS detector used was unable to detect carbon). It can be seen that the fine plate-shaped grains and coarse blocky grains had uniform distribution of Si and Ti suggesting these phases as Ti_3SiC_2. The bright agglomerates were rich in Al. EDS spot analysis of these bright agglomerates indicated presence of both Ti and Si peaks along with Al, suggesting formation of $Ti_3(Si_{1-x}Al_x)C_2$ solid solution. For the Ti_3SiC_2–TiC composite samples, the microstructure mainly consisted of plate-shaped fine Ti_3SiC_2 grains, coarse TiC grains, and Al-rich bright agglomerates. In the previous work on Ti_3SiC_2–TiC composites, observed volume fraction of TiC reinforcement (calculated from XRD analysis) was found to be lower than that predicted from stoichiometric calculations [18,19]. This is quite unusual as TiC

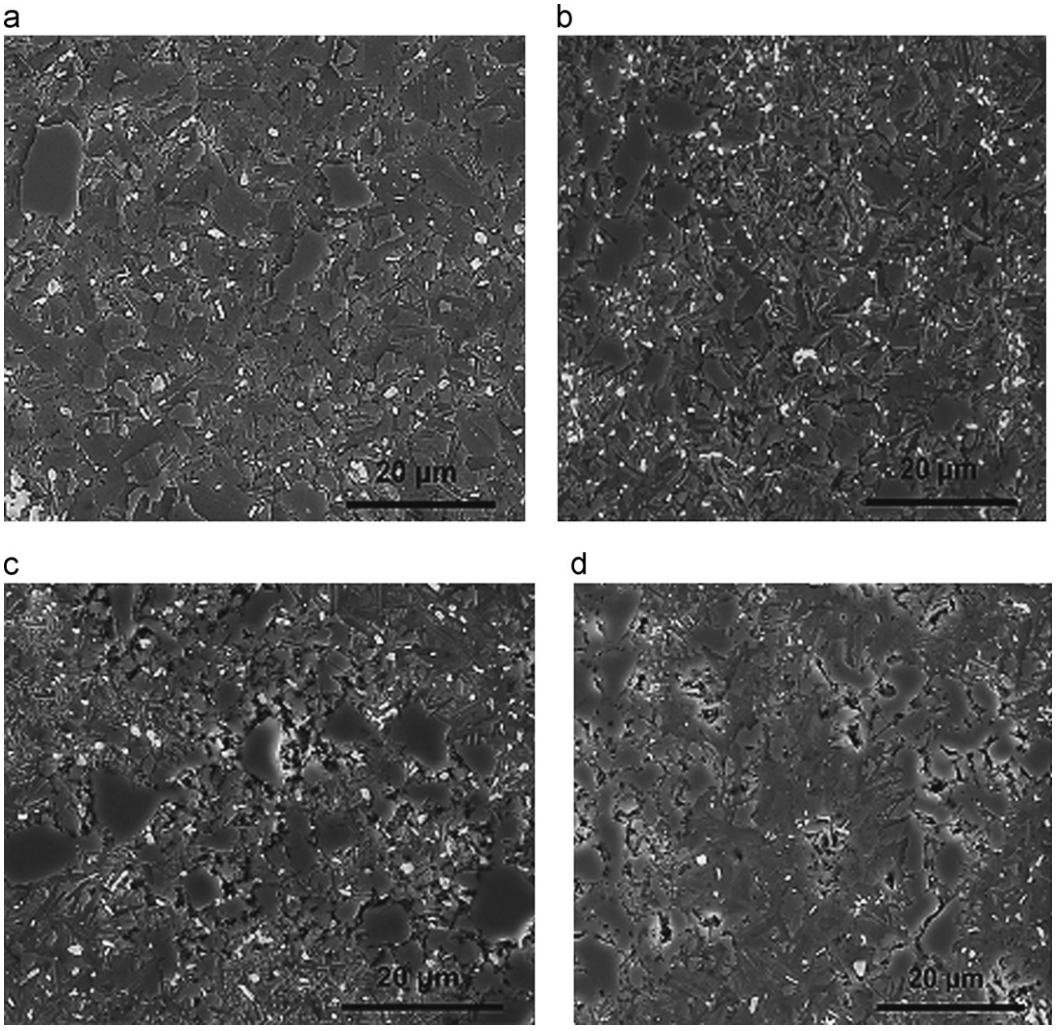

Fig. 5. SEM micrographs from the polished and etched surfaces of Ti_3SiC_2–TiC composites: (a) TSC, (b) TC10, (c) TC20, and (d) TC30 samples.

can always be present as a starting constituent, intermediate phase, or decomposition product of Ti_3SiC_2. This discrepancy between the observed and desired TiC reinforcement content is possibly due to the formation of partial solid solution. The amount of plate-shaped grains decreases and the coarse TiC grains become increasingly distinct with increasing TiC reinforcement content in the composites (Fig. 5b–d). While the TiC grains appear well distributed at lower reinforcement content (10–20 vol% TiC), the coarse TiC grains form agglomerates at higher TiC reinforcement content (30 vol%). Distributed porosity, in agreement with the relative density data, can also be seen in the microstructures of heavily reinforced Ti_3SiC_2–TiC composites.

3.3. Microhardness and wear behavior

Fig. 7 presents the variation of Vickers microhardness of Ti_3SiC_2–TiC composites with TiC reinforcement content. The microhardness of the composites increased almost linearly with increasing TiC reinforcement content. The hardness of TiC (28–30 GPa) is nearly 7–8 times the previously reported values of hardness of Ti_3SiC_2 (4 GPa). For the nearly single phase Ti_3SiC_2 (sample TSC) SPS sintered in this investigation, the microhardness was found to be 5.96 ± 0.19 GPa (measured with indentation load of 9.8 N), which is higher than the previously reported hardness values for monolithic Ti_3SiC_2 [23]. While the higher hardness of the TSC sample could be due to minor amount of TiC phase in the TSC sample, it could also be due to indentation size effects. El Raghy et al. observed very strong indentation size effects on hardness [6]. It was reported that the hardness decreases with increasing load and asymptotes to a value of 4 GPa at higher loads. The microhardness in the range of about 7–9 GPa was reported for lower loads ($\sim$1 N). The Ti_3SiC_2–TiC composites reinforced with 30 vol% TiC (TC30) exhibited highest hardness of about 9.32 ± 0.37 GPa. While this hardness value of the composite is consistent with the earlier reports by Tian et al. [18] and Ho-Duc et al. [15], it is nearly 2 GPa lower than that reported by Zhang et al. [17]. As the hardness of Ti_3SiC_2–TiC

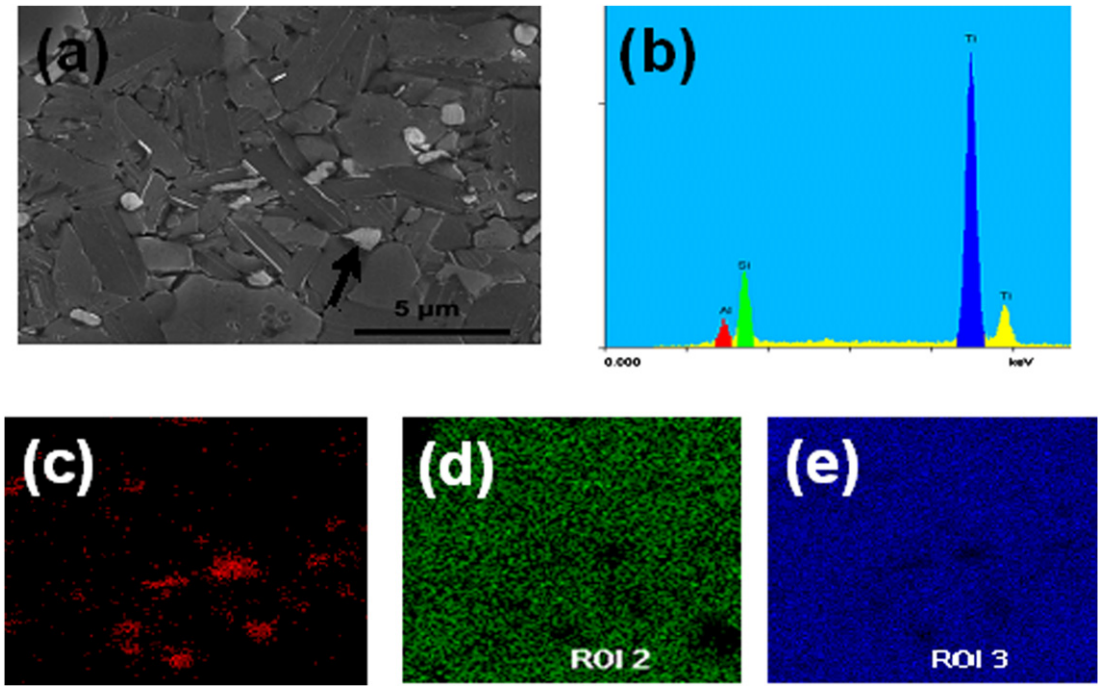

Fig. 6. (a) SEM micrograph from TSC sample, (b) EDS of bright precipitate indicated by an arrow on (a) and (c–e) EDS mapping of Al, Si, and Ti, respectively.

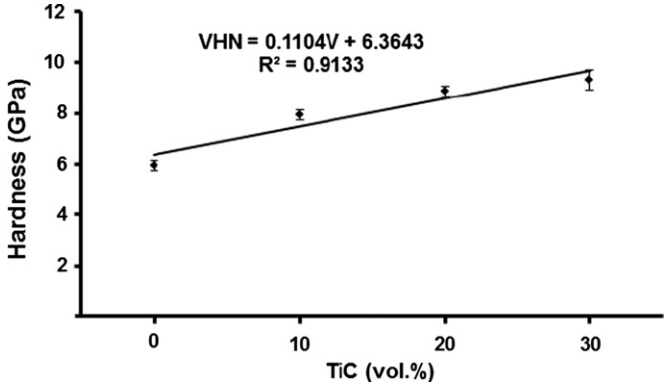

Fig. 7. Vickers microhardness of Ti_3SiC_2–TiC composites as a function of TiC reinforcement content.

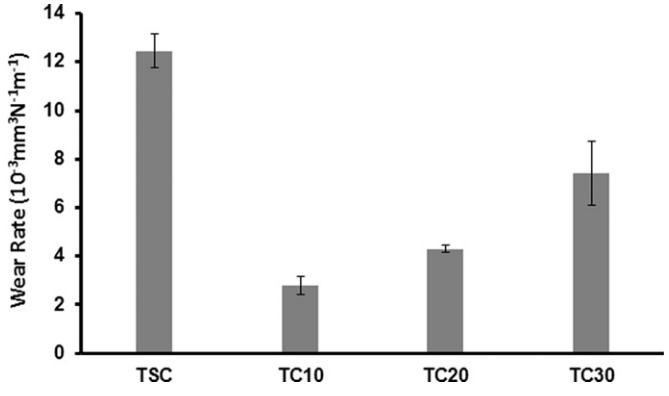

Fig. 8. Dry sliding wear rates for Ti_3SiC_2 (TSC) and Ti_3SiC_2–TiC (TC10, TC 20, and TC30) composites against Si_3N_4 ball for a load of 10 N.

composites increases almost linearly with TiC reinforcement content, a least-squares fit can be obtained as:

$$VHN = 6.3643 + 0.1104V, \quad (3)$$

where VHN is microhardness in GPa and V is amount of TiC reinforcement in vol%. The correlation parameter of data fitting (R^2) for this relationship is 0.9133 Fig. 8.

Fig. 9 presents the dry sliding wear rates, measured using ball-on-disc wear set-up, for Ti_3SiC_2 (TSC) and Ti_3SiC_2–TiC (TC10, TC 20, and TC30) composites. Among all the compositions, the TSC samples exhibited highest sliding wear rate of $1.2 \times 10^{-2}\,mm^3\,N^{-1}\,m^{-1}$. The wear rate for all Ti_3SiC_2–TiC composites was significantly less than that for Ti_3SiC_2 indicating improvement in wear resistance with TiC reinforcement in Ti_3SiC_2 matrix. The composites reinforced with 10 vol% TiC showed least wear rate (best wear resistance) among composites compositions investigated. For the given wear testing parameters, the wear rates for TC10, TC20, and TC30 were $2.7 \times 10^{-3}\,mm^3\,N^{-1}\,m^{-1}$, $4.3 \times 10^{-3}\,mm^3\,N^{-1}\,m^{-1}$, and $7.4 \times 10^{-3}\,mm^3\,N^{-1}\,m^{-1}$, respectively. The depth profiles across the wear tracks for the Ti_3SiC_2 (TSC) and Ti_3SiC_2–TiC (TC10, TC 20, and TC30) composites are also shown in Fig. 10. While the average width of the wear tracks was not significantly different among Ti_3SiC_2 and composite samples, the average depth of wear tracks followed similar trend as the wear rate for sintered samples. The depth of wear track was highest (~38 μm) for Ti_3SiC_2 samples. Among the Ti_3SiC_2–TiC composites, the TC10 samples reinforced with 10 vol% TiC exhibited lowest depth of wear track (~10 μm). The depth of wear track further increases with increasing TiC content

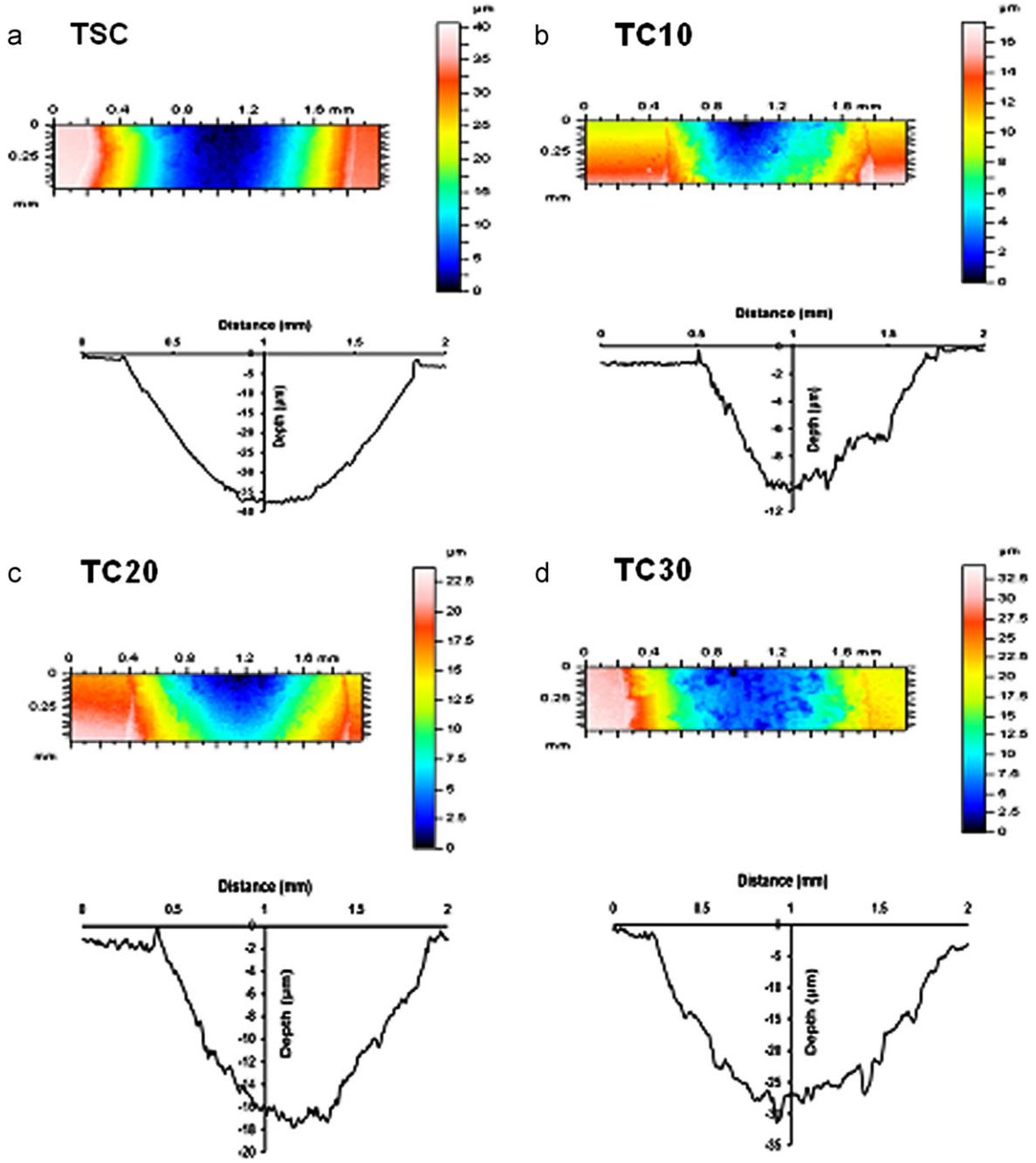

Fig. 9. Surface and depth profiles across the wear tracks: (a) TSC (Ti_3SiC_2), (b) TC10, (c) TC20, and (d) TC30 Ti_3SiC_2–TiC composites.

(TC20 and TC30). The depths of wear tracks were about 18 and 30 μm for composites reinforced with 20 and 30 vol% TiC, respectively. While the TSC samples exhibited least wear resistance (indicated by highest wear rate and depth of wear track), the wear response of the composites with increasing TiC content did not follow similar trend as the hardness of the composites. The TC10 composites (reinforced with 10 vol% TiC) showed best wear resistance in spite of lowest hardness among the composites. The variation of coefficient of friction (COF) during all the 10 min intervals of each wear test (total test time of 1 h) for the Ti_3SiC_2 and Ti_3SiC_2–TiC composites is shown in Fig. 10. For all the samples, the COF stabilized at some average value during entire duration of wear tests indicating steady state wear regime (linear wear volume loss). The average COF for TSC samples (~0.70–0.75) was slightly greater than that for Ti_3SiC_2–TiC composites (0.60–0.65). The reinforcement of hard TiC phase in Ti_3SiC_2 matrix seems to decrease accumulative strain and strain energy and decentralize the shear stress at the contact points, resulting in relatively lower COF for the composites.

SEM micrographs from the surfaces of wear tracks of Ti_3SiC_2 and Ti_3SiC_2–TiC composite samples are presented in Fig. 11. The Ti_3SiC_2 samples showed pronounced grain fracture and detachment. The bending and fracture of lamellar

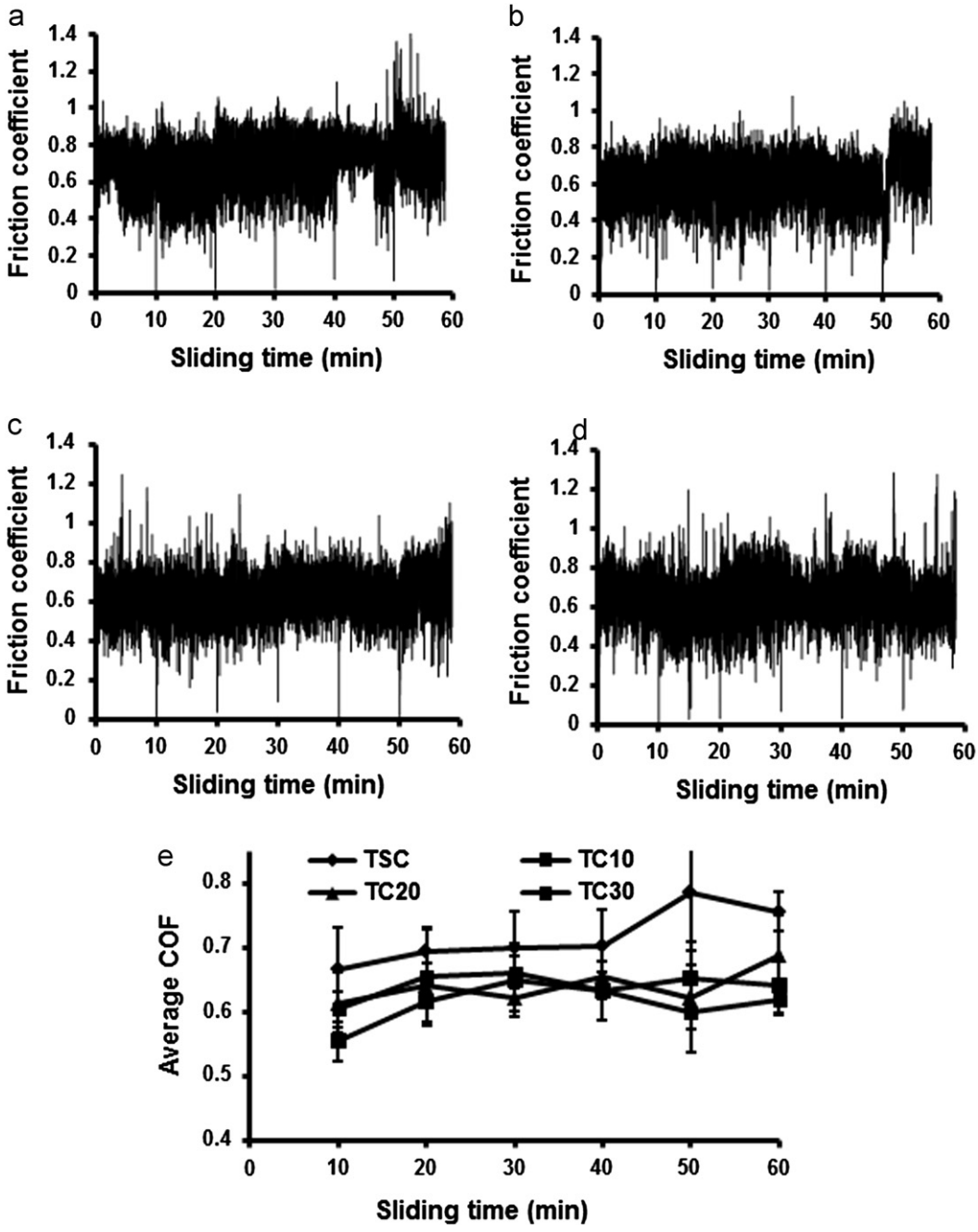

Fig. 10. (a–d) Friction coefficients as a function of sliding time for TSC, TC10, TC20, and TC30 samples, respectively; and (e) comparison of average friction coefficients as a function of sliding time for all samples.

grains can be readily seen in the micrograph (Fig. 11a). A high magnification image from these wear surfaces indicated significant cracking leading away from the debris-filled depressions, the regions of grain fracture and detachment (Fig. 11b). The wear surface of the Ti_3SiC_2 samples appears relatively rougher due to these debris-filled depressions, and this is possibly the reason for relatively higher COF for these samples. In the previous report, Wan et al. showed that the pulled-out grain particles get transferred to the counterpart surface, suggesting adhesive wear as an active wear mechanism for Ti_3SiC_2 samples [24]. For Ti_3SiC_2–TiC with 10 vol% TiC, the wear surface is relatively flatter. The microstructure of the wear surface clearly indicates higher wear loss for the matrix phase while the flattened coarse grains of hard TiC phase remain protruded out of the wear surface (Fig. 11c). The micro-scratching and micro-cracking of the flattened TiC phase regions indicate abrasive wear. Thus, the Ti_3SiC_2–TiC composites 10 vol% TiC exhibit complex adhesive and abrasive mechanisms corresponding to matrix and reinforcement phases, respectively. Improved wear resistance was also reported for $Ti_3Si(Al)C_2$/SiC [24], Ti_3SiC_2/(TiC+TiB_2) [9], and Ti_3SiC_2/Al_2O_3 [25] composites by the similar mechanisms.

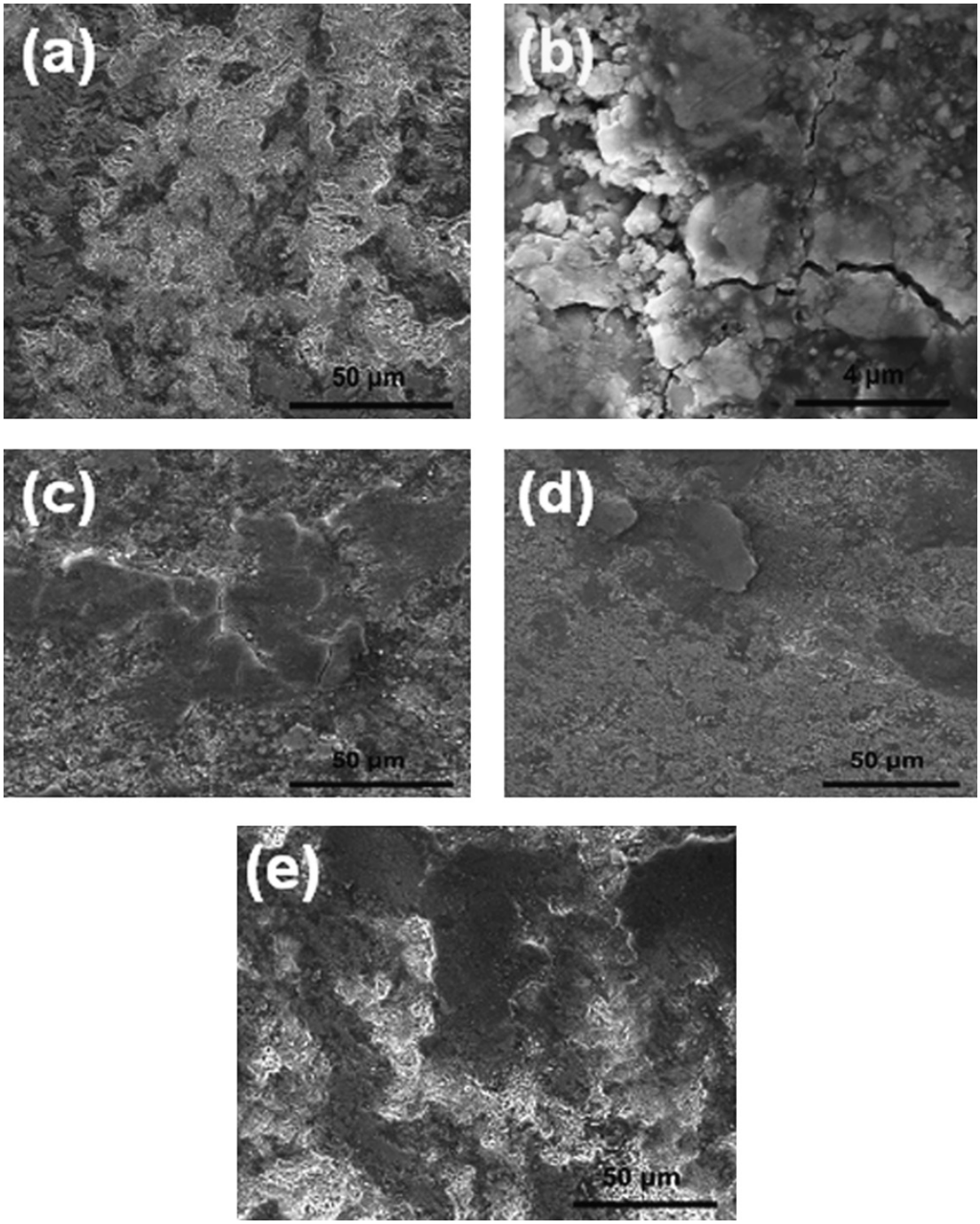

Fig. 11. SEM micrographs from the worn surfaces of (a and b) TSC (Ti_3SiC_2), (c) TC10, (d) TC20, and (e) TC30 Ti_3SiC_2–TiC composites.

It was also reported that the wear loss of the composites decreases with increasing amount of SiC and Al_2O_3 reinforcement [24,25]. Hu et al. demonstrated using FEM analysis that the presence of hard reinforcing particles, such as Al_2O_3, can effectively decentralize the shear stress under the counterpart and improve the wear resistance of the composites [26]. In the present study, the wear rate increases with increasing TiC reinforcement content in the composites, even though there is an increase in hardness associated with increasing TiC reinforcement. When ceramics slide against ceramics, fracture toughness becomes relatively more important than hardness in determining the wear resistance as the wear volume loss in ceramics occurs primarily due to fracture rather than plastic deformation [26,27]. Fischer et al. reported that wear resistance of yttria-doped zirconium oxide increases with the fourth power of its fracture toughness [28]. The SEM micrographs (Fig. 5) reinforced with higher reinforcement content (20–30 vol% TiC) showed non-uniform distribution of TiC phase in the matrix. The fracture toughness of Ti_3SiC_2–TiC (30 vol%) composites where TiC distribution was non-uniform was reported to be 5.5 ± 0.5 MPa $m^{1/2}$, which is significantly lower than that reported for the monolithic

Ti_3SiC_2 (8–16 MPa $m^{1/2}$) [15,29]. The presence of agglomerated TiC phase regions in the microstructure decreases the fracture toughness and degrades the wear resistance of the composites reinforced with higher TiC content [30]. Note that the samples with higher TiC reinforcement content also had some porosity. The porosity weakens the interfaces between the matrix phase and the reinforcing phase causing easy pull-out/detachment of the hard grains under dry sliding wear conditions. The released hard particles can initiate additional three-body wear mechanisms resulting in severe wear. SEM micrographs from the wear surfaces of Ti_3SiC_2–TiC composites reinforced with 20 and 30 vol% TiC clearly indicate severe wear of the matrix and islands of detaching TiC phase regions (Fig. 11d and e).

4. Conclusions

Ti_3SiC_2 and Ti_3SiC_2–TiC composites (reinforced with up to 30 vol% TiC) have been successfully processed from TiC/Si/Ti/Al powder mixtures using spark plasma sintering (SPS) at 1250 °C. Additional TiC content, in excess of stoichiometric TiC required for Ti_3SiC_2 matrix formation, in the starting powder mixtures determines the level of reinforcement in the sintered Ti_3SiC_2–TiC composites. The TiC content in the sintered composites, calculated from XRD analysis, is fairly close to the theoretical TiC content based on stoichiometry. For the similar SPS processing parameters, the relative density of the sintered composites decreased with increasing TiC reinforcement content. While the distribution of TiC in the composites was uniform at lower reinforcement content (10 vol%), the agglomeration of TiC phase regions was observed for composites reinforced with 20 and 30 vol% TiC. All the Ti_3SiC_2–TiC composites (with 10–30 vol% TiC) showed higher hardness and better wear resistance compared to Ti_3SiC_2. Even though the hardness of Ti_3SiC_2–TiC composites increased almost linearly with the increasing reinforcement content (0–30 vol%), the composites reinforced with 10 vol% TiC exhibited best wear resistance among the investigated compositions. Dry sliding wear of the composites seems to be dominated by adhesive material transfer from the Ti_3SiC_2 matrix and the fracture with grain detachment of the hard TiC phase regions depending on the reinforcement content of the composites.

References

[1] M. Radovic, A. Ganguly, M.W. Barsoum, T. Zhen, P. Finkel, S.R. Kalidindib, E. Lara-Curzioa, On the elastic properties and mechanical damping of Ti_3SiC_2, Ti_3GeC_2, $Ti_3Si_{0.5}Al_{0.5}C_2$ and Ti_2AlC in the 300–1573 K temperature range, Acta Materialia 54 (2006) 2757–2767.

[2] P. Finkel, M.W. Barsoum, T. El-Raghy, Low temperature dependence of the elastic properties of Ti_3SiC_2, Journal of Applied Physics 85 (1999) 7123–7126.

[3] M.W. Barsoum, T. El-Raghy, C.J. Rawn, W.D. Porter, A. Payzant, C. Hubbard, Thermal properties of Ti_3SiC_2, Journal of Physics and Chemistry of Solids 60 (1999) 429–439.

[4] M.W. Barsoum, T. El-Raghy, The MAX phases: unique new carbide and nitride materials, American Scientist 89 (2001) 334–343.

[5] S. Myhra, J.W.B. Summers, E.H. Kisi, Ti_3SiC_2—a layered ceramic exhibiting ultra-low friction, Materials Letters 39 (1999) 6–11.

[6] T. El-Raghy, P. Blau, M.W. Barsoum, Effect of grain size and wear behavior of Ti_3SiC_2, Wear 238 (2000) 125–130.

[7] H.J. Wang, Z.H. Jina, Y. Miyamotob, Ti_3SiC_2/Al_2O_3 composites prepared by SPS, Ceramics International 29 (2003) 539–542.

[8] W. Pan, S.L. Shia, Microstructure and mechanical properties of Ti_3SiC_2/3Y-TZP composites by spark plasma sintering, Journal of the European Ceramic Society 27 (2007) 413–417.

[9] J. Yang, W. Gu, L.M. Pan, K. Song, X. Chen, T. Qiu, Friction and wear properties of in situ (TiB_2+TiC)/Ti_3SiC_2 composites, Wear 271 (2011) 2940–2946.

[10] J. Zhang, L. Wang, L. Shi, W. Jiang, L. Chena, Rapid fabrication of Ti_3SiC_2–SiC nanocomposite using the spark plasma sintering-reactive synthesis (SPS-RS) method, Scripta Materialia 56 (2007) 241–244.

[11] J. Zhang, T. Wua, L. Wang, W. Jiang, L. Chen, Microstructure and properties of Ti_3SiC_2/SiC nanocomposites fabricated by spark plasma sintering, Composites Science and Technology 68 (2008) 499–505.

[12] Z.F. Zhang, Z.M. Sun, H. Hashimoto, Rapid synthesis of ternary carbide Ti_3SiC_2 through pulse-discharge sintering technique from Ti/Si/TiC powders, Metallurgical and Materials Transactions A 33 (2002) 3321–3328.

[13] H.O. Pierson, Handbook of Refractory Carbides and Nitrides, Noyes Publications, Westwood, NJ, 1996.

[14] D.T. Wan, Y.C. Zhou, Y.W. Bao, C.K. Yan, In-Situ reaction synthesis and characterization of $Ti_3Si(Al)C_2$/SiC composites, Ceramics International 32 (2006) 883–890.

[15] L.H. Ho-Duc, T. El-Raghy, M.W. Barsoum, Synthesis and characterization of 0.3 Vf TiC–Ti $_3SiC_2$ and 0.3 Vf SiC–Ti $_3SiC_2$ composites, Journal of Alloys and Compounds 350 (2003) 303–312.

[16] H. Hashimoto, Z.M. Sun, Preparation of TiC–Ti $_3SiC_2$ composites by mechanical alloying and hot pressing, Materials Transactions 49 (2008) 1572–1578.

[17] J.F. Zhang, L.J. Wang, W. Jiang, L.D. Chen, Effect of TiC content on the microstructure and properties of Ti_3SiC_2–TiC composites in situ fabricated by spark plasma sintering, Materials Science and Engineering A 487 (2008) 137–143.

[18] W. Tian, Z.M. Sun, Hitoshi Hashimotoa, YuLei Dua, Synthesis, microstructure and mechanical properties of Ti_3SiC_2–TiC composites pulse discharge sintered from Ti/Si/TiC powder mixture, Materials Science and Engineering 526 (2009) 16–21.

[19] W. Tian, Z. Sun, H. Hashimoto, Y. Du, Microstructural evolution and mechanical properties of Ti_3SiC_2–TiC composites, Journal of Alloys and Compounds 502 (2010) 49–53.

[20] J. Zhu, B. Mei, X. Xu, J. Liu, Synthesis of single-phase polycrystalline Ti_3SiC_2 and Ti_3AlC_2 by hot pressing with the assistance of metallic Al or Si, Materials Letters 58 (2004) 588–592.

[21] S. yang, Z.M. SUN, H. Hashimoto, Reaction in Ti_3SiC_2 powder synthesis from a Ti–Si–TiC powder mixture, Journal of Alloys and compounds 368 (2004) 312–317.

[22] A. Teber, F. Schonstein, F. Tetard, M. Abdellaoui, N. Jouini, Effect of SPS process sintering on the microstructure and mechanical properties of nanocrystalline TiC for tools application, International Journal of Refractory Metals and Hard Materials 30 (2012) 64–70.

[23] T. El-Raghy, P. Blau, M.W. Barsoum, Effect of grain size and wear behavior of Ti_3SiC_2, Wear 238 (2000) 125–130.

[24] D.T. Wan, C.F. Hu, Y.W. Bao, Y.C. Zhou, Effect of SiC particles on the friction and wear behavior of $Ti_3Si(Al)C_2$-based composite, Wear 262 (2007) 826–832.

[25] C. Hu, Y. Zhou, Y. Bao, D. Wan, Tribological properties of polycrystalline Ti_3SiC_2 and Al_2O_3 reinforced Ti_3SiC_2 composite, Journal of the American Ceramic Society 89 (2006) 3456–3461.

[26] A.G. Evans, D.B. Marshall, Wear mechanisms in ceramics in: D.A. Rigney (Ed.), Fundamentals of Friction and Wear of Materials, American Society for Metals, Metals Park, OH, 1980, pp. 439–452.

[27] T.E. Fischer, H. Tomizawa, Interaction of microfracture and tribochemistry in the friction and wear of silicon nitride, Wear 105 (1985) 29–45.
[28] T.E. fisher, M.P. Anderson, S. jahanmir, Influence of fracture toughness on the wear resistance of yttria-doped zirconium oxide, Journal of the American Ceramic Society 72 (1989) 252–257.
[29] C.J. Gilbert, D.R. Bloyer, M.W. Barsoum, T. El-Raghy, A.P. Tomsia, R.O. Ritchie, Fatigue-crack growth and fracture properties of coarse and fine-grained Ti_3SiC_2, Scripta Materialia 42 (2000) 761–767.
[30] K.H. Zum Gahr, How microstructure affects abrasive wear resistance, Metal Progress 116 (1979) 46–52.